View metadata, citation and similar papers at core.ac.uk

brought to you by CORE

provided by Elsevier - Publisher Connector

ELSEVIER

Available at
www.ElsevierMathematics.com
POWERED BY SCIENCE DIRECT®

Journal of Computational and Applied Mathematics 163 (2004) 319–331

JOURNAL OF COMPUTATIONAL AND APPLIED MATHEMATICS

www.elsevier.com/locate/cam

Numerical simulation of gas-particle flow in a single-side backward-facing step flow

K.F. Yu[a,*], K.S. Lau[a], C.K. Chan[b]

[a] *Department of Applied Physics, The Hong Kong Polytechnic University, Hong Kong, China*
[b] *Department of Applied Mathematics, The Hong Kong Polytechnic University, Hong Kong, China*

Received 30 November 2002; received in revised form 9 June 2003

Abstract

Particle-laden turbulent flow over a backward-facing step has been investigated by using large eddy simulation for the fluid phase while particle motion is traced by particle track model. Effects of both drag and gravitational forces on particle motion are considered. The simulation is carried out with the flow parameters and geometry of the test section is same as those in the experiment carried out by Fessler and Eaton (J. Fluid Mech. 314 (1999) 97), who measured the two-dimensional flow fields of both phases. Predicted statistical mean properties of the fluid phase with Reynolds number of 18,400 and particle phase with 70 μm copper spheres and 150 μm glass spheres respectively are in good agreement with the experimental results. Simulation also predicts detailed flow fields of both phases and their evolution. Further investigation has been carried out on the dispersion of particles with different Stokes numbers in the turbulent structure of the fluid field. Motion of glass spheres with diameters 2, 20, 50, 100 and 200 μm, respectively, introduced in the fluid field is simulated. The predicted patterns of instantaneous dispersion of particles reveal that the phenomenon of preferential concentration of particles occurs at a certain range of Stokes number. The effects of initial velocity slip between the two phases and the action of gravity on particle dispersion are also investigated.
© 2003 Elsevier B.V. All rights reserved.

MSC: 76F65; 76T15; 76F05

Keywords: Large eddy simulation; Backward-facing step; Particle-laden flow; Turbulent flow

1. Introduction

Turbulence is a phenomenon that occurs frequently in nature. It has been the subject of study for over 100 years. In present days, the prediction and control of turbulent flows have become

* Corresponding author.
E-mail address: 02900925r@polyu.edu.hk (K.F. Yu).

0377-0427/$ - see front matter © 2003 Elsevier B.V. All rights reserved.
doi:10.1016/j.cam.2003.08.077

increasingly important, especially for particle-laden turbulent flows, due to their frequent occurrence in technological applications involving industrial systems, energy conversion systems and geophysical applications. Describing and predicting the turbulent characteristics of particle-laden flows is therefore an important research topic in applied fluid mechanics.

Traditional approaches of computational studies are usually based on the Reynolds-averaged Navier–Stokes (RANS) equations in which the turbulent spectrum is parameterized by semi-empirical turbulence modeling. A primary shortcoming of RANS methods is that the effect of large-scale vortical structures and distortion of turbulent eddies is not taken into account. Direct numerical simulation (DNS) is one of the approaches to overcome this. In DNS, the Navier–Stokes equations are solved directly without introducing any model and hence the process consumes a huge computer time even for flows of moderately large Reynolds number.

Large eddy simulation (LES) offers the advantages of calculating directly the large-scale energy containing motion and modeling the small-scale energy dissipating motion. So, LES predictions have less computational time compared with DNS and less modeling errors compared with RANS. In a previous simulation [3] of the same configuration and flow parameters as those in the experimental work of Fessler and Eaton [6] using Reynolds-averaged equations with the k–ε model and the improved stochastic separated flow model, only time averages of the flow fields and the particle density were predicted. The present work not only provides the evolution of the flow fields but reveals finer details of the flow pattern. It predicts, for example, a small anti-clockwise recirculation region near the corner between the step and the lower wall. This region has not been predicted by previous simulation using RANS [3], nor resolvable in the experimental work of Fessler and Eaton [6].

2. Configuration of simulation

Fig. 1 shows a schematic diagram of the test section of the experiment carried out by Fessler and Eaton [6]. The width of the section in the z-direction perpendicular to the paper is much larger than that in the y-direction so that the flow can be considered as two dimensional. The backward-facing step has an expansion ratio of 5:3. Reynolds number of the air flow over the backward-facing step is 18,400, based on the maximum inlet velocity of 10.5 m s^{-1} and step height 26.7 mm. Particles introduced into the flow are glass spheres of diameter 150 μm, density 2500 kg m^{-3} and copper spheres of diameter 70 μm, density 8800 kg m^{-3} respectively. Numerical simulation is carried out with the same flow parameters and geometry as those of the experiment, except that the length of the backward step channel is doubled in order to observe the fully developed flow. Predicted results

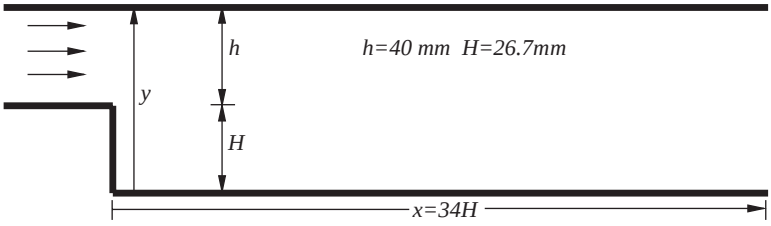

Fig. 1. Schematice diagram of test section.

of velocity of both phases agree well with the experimental data. In order to investigate further the effect of particle parameters on particle–vortex interaction, hypothetical glass spheres with different diameters, 2, 20, 50, 100 and 200 μm are introduced into the flow and the simulated results are then computed and compared.

3. Continuous phase equations

LES is used to simulate the gas phase of the flow. The flow field variables are separated into a large-scale component and a subgrid scale (SGS) component by filtering. The effect of the subgrid scales on the resolved scales is modeled by the SGS stress according to the Smagorinsky model [8]. The space filtered time-dependent incompressible Navier–Stokes equations with Smagorinsky model in Cartesian coordinates can then be written as

$$\frac{\partial \rho u_i}{\partial x_i} = 0, \tag{1}$$

$$\frac{\partial \rho u_i}{\partial t} + \frac{\partial \rho u_i u_j}{\partial x_j} = -\frac{\partial p}{\partial x_i} + \frac{\partial}{\partial x_j}\left[\mu^*\left(\frac{\partial u_i}{\partial x_j} + \frac{\partial u_j}{\partial x_i}\right)\right], \tag{2}$$

where $\mu^* = \mu/Re + \mu_T$, Re is the Reynolds number of fluid phase, μ is the molecular viscosity and μ_T is eddy viscosity given by $\mu_T = \rho(C_s\Delta)^2|S| = (C_s\Delta)^2\sqrt{2S_{ij}S_{ij}}$. S_{ij} is the rate of strain tensor of the filtered velocity field, $\Delta = \sqrt{\Delta x \Delta y}$ is the filter width, and $C_s = 0.048$ is chosen as the Smagorinsky model parameter. The equations have been nondimensionalized using the step height as the length scale, the maximum inlet velocity as the velocity scale and the ratio of the step height and maximum inlet velocity as the time scale.

The governing equations are discretized spatially on a staggered Cartesian grid. In the current study, a uniform grid with 259 nodes in the streamwise x-direction and 25 nodes in the transverse y-direction is used. Derivatives are approximated using central difference for the diffusion terms while the advection terms are discretized by an upwind scheme. Time integration of the governing equations is done with a second-order Adams–Bashforth scheme. The time step is taken as 0.005. Chorin's [4] fractional-step projection method is adopted in solving the incompressible gas-phase equations. The Poission equation for pressure correction is formed and solved directly using the Buneman variant of cyclic odd–even reduction algorithm [2].

The initial velocity condition of simulation is simply set as the inlet velocity profile obtained from the experimental data. This initial condition will be 'forgotten' after a number of iterations as mentioned by other researcher [11]. No initial inflow pressure condition is imposed. The simulation results show that using these initial conditions, does not affect the validity of our predictions. At all solid boundaries, velocity and pressure gradient are set as zero. At the outflow boundary, a convective open boundary condition [1] is used while the pressure is also left free.

4. Particle phase equations

The flow field of the particles is simulated and visualized when fluid phase has become steady. Twenty particles are evenly spaced along the inlet and added at intervals of 10 time steps. There are

totally 80,000 particles introduced into the backward facing step channel at the end of the simulation. Lagrangian approach is employed to predict the properties of each particle directly from the equations of motion. The basic assumptions for the particle motion are:

(1) All particles are rigid spheres with equal diameter and density.
(2) The density of the particles is assumed large compared with that of the fluid.
(3) Particle–particle interactions are negligible.
(4) Dilute two-phase particle-laden flow is assumed and the effect of the particles on the flow structures is neglected.
(5) Collisions with boundaries are assumed to be elastic.

The governing equations for a particle along its trajectory with drag and gravitational forces can be written as

$$\frac{\mathrm{d}\vec{x}_\mathrm{p}}{\mathrm{d}t} = \vec{u}_\mathrm{p}, \tag{3}$$

$$\frac{\mathrm{d}\vec{u}_\mathrm{p}}{\mathrm{d}t} = \frac{\vec{f}^{\,\mathrm{drag}}}{m_\mathrm{p}} + \vec{g}, \tag{4}$$

where $\vec{u}_\mathrm{p}$ is the instantaneous particle velocity, $\vec{x}_\mathrm{p}$ is the displacement of particle, m_p is the mass of particle, $\vec{f}^{\,\mathrm{drag}}$ is the drag force and $\vec{g}$ is the gravitational acceleration.

The drag [5] and gravitational force of a single particle in a uniform flow field can be generally expressed by

$$\vec{f}^{\,\mathrm{drag}} = C_\mathrm{d}\,\tfrac{1}{4}\,\pi d_\mathrm{p}^2\,\frac{\rho_\mathrm{f}}{2}\,|\vec{u}_\mathrm{f} - \vec{u}_\mathrm{p}|(\vec{u}_\mathrm{f} - \vec{u}_\mathrm{p}), \tag{5}$$

where d_p the diameter of the particle respectively, ρ_f and $\vec{u}_\mathrm{f}$ is the density and diameter of the fluid, respectively, and C_d is the drag coefficients [6] given by

$$C_\mathrm{d} = \frac{24}{Re_\mathrm{p}}\,(1 + 0.15Re_\mathrm{p}^{0.687}) \quad \text{for } Re_\mathrm{p} \leqslant 700 \tag{6}$$

with the particle Reynolds number [5] is defined by

$$Re_\mathrm{p} = \frac{\rho_\mathrm{f}|\vec{u}_\mathrm{f} - \vec{u}_\mathrm{p}|(\vec{u}_\mathrm{f} - \vec{u}_\mathrm{p})}{\mu_\mathrm{f}}. \tag{7}$$

5. Results and discussions

5.1. Velocity profile of fluid phase

Fig. 2 shows the predicted streamwise mean velocity profiles and the corresponding experimental data of the gas phases at different downstream position $x/H = 2$, 5, 7, 9 and 14. Simulation results are in good agreement with those obtained from the experiment of Fessler and Eaton [6] with Reynolds number of 18,400. Fig. 3 shows the predicted mean streamline flow pattern. The predicted reattachment length of $7.41H$ agrees well with the experimental value of $7.4H$. Simulation also predicts a small anti-clockwise circulation region near the corner between the step and the lower wall.

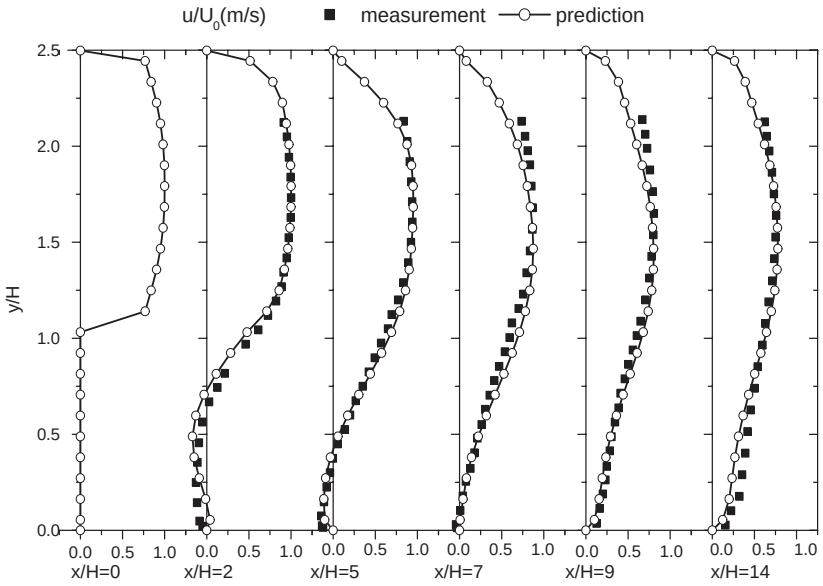

Fig. 2. Streamwise mean velocity (gas phase).

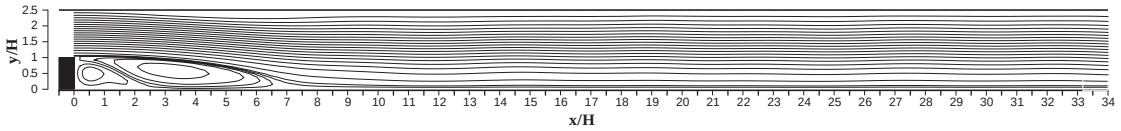

Fig. 3. Mean streamline flow pattern (gas phase).

This secondary circulation region has length $2.38H$ in x-direction, and height $0.81H$ in y-direction. This region has not been reported in the experiment work of Fessler and Eaton [6] nor predicted by simulation using Reynolds-averaged equations [3], but observed in other numerical work with different Reynolds number [7].

5.2. Velocity profiles for glass and copper particle

For validation of the particle phase, two classes of 150 μm glass and 70 μm copper particles are used. The glass and copper particles chosen have similar Stokes number of 6.9 and 7.2, respectively, but different diameters. In this numerical simulation, the initial velocities are equal to 92% and 88% of those of the fluid phase for glass and copper particles, respectively, according to the experimental finding by Fessler and Eaton [6].

Figs. 4 and 5 show the streamwise mean velocity for glass and copper spheres respectively. The predicted values agree well with those of the experiment by Fessler and Eaton [6].

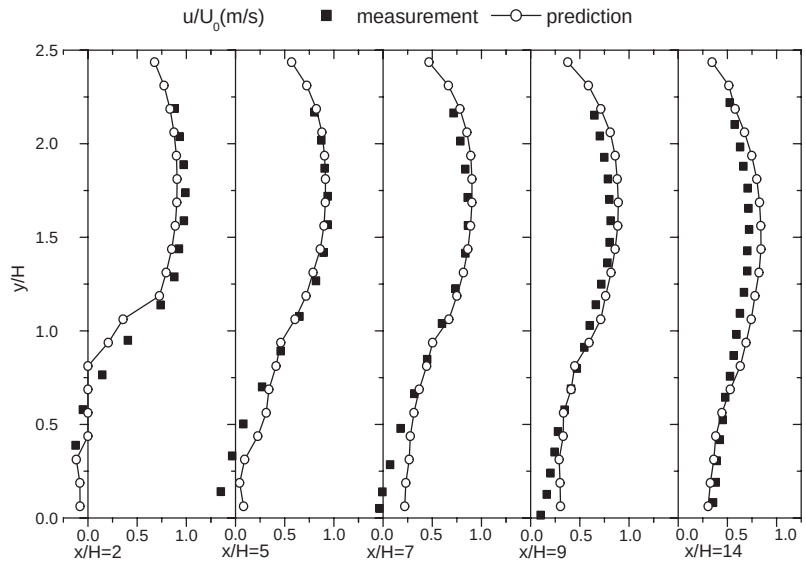

Fig. 4. Streamwise mean velocity for 150 μm glass particle.

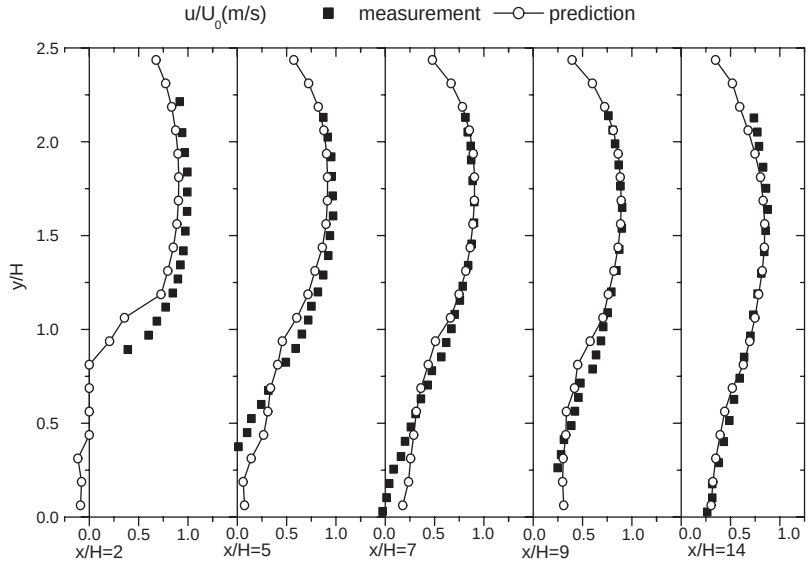

Fig. 5. Streamwise mean velocity for 70 μm copper particle.

5.3. *Effect of Stokes number on particle behaviors*

The Stokes number used to characterize the motion of selected particle is defined as the ratio of the particle dynamic relaxation time (τ_p) to the gas time scale (τ_f) in the flow. According to the

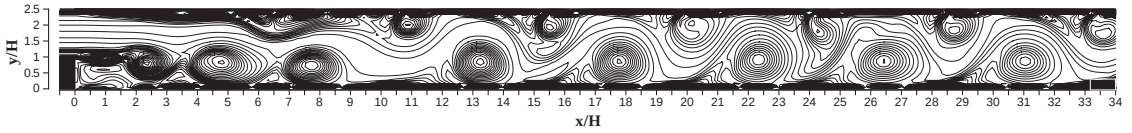

Fig. 6. Vorticity contours of the gas phase.

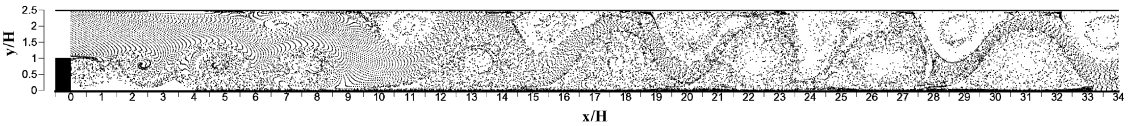

(a) 2μm particles, Stokes number 0.002

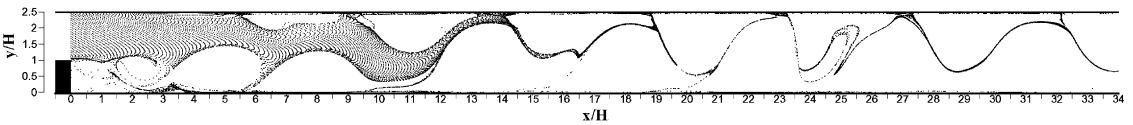

(b) 20μm particles, Stokes number 0.2

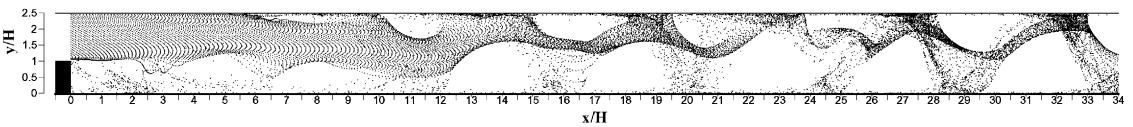

(c) 50μm particles, Stokes number 1.06

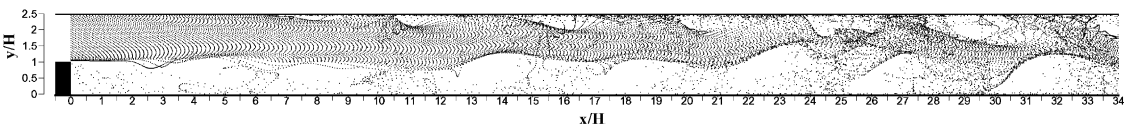

(d) 100μm particles, Stokes number 3.7

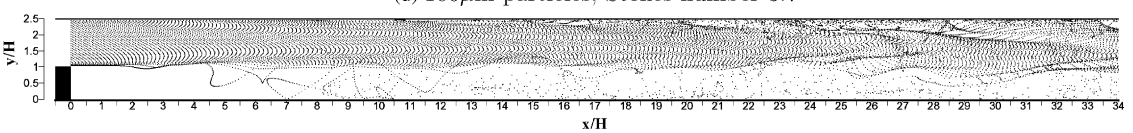

(e) 200μm particles, Stokes number 11.9

Fig. 7. Particle distribution with different Stokes number. (a) 2 μm particles, Stokes number 0.002; (b) 20 μm particles, Stokes number 0.2; (c) 50 μm particles, Stokes number 1.06; (d) 100 μm particles, Stokes number 3.7; (e) 200 μm particles, Stokes number 11.9.

experiment of Fessler and Eaton [6], $\tau_p = \rho_p d_p^2/18\mu_f$, an average slip velocity of 1.2 m^{-1} is assumed to calculate the particle Reynolds number and $\tau_f = 5H_0/U_0$, based on an approximate large-eddy passing frequency in the separated shear layer. Glass spheres of the same size are introduced into the flow when simulation result of the gas phase becomes steady (after 300 nondimensional time). The diameters of particles are 2, 20, 50, 100 and 200 μm, respectively. The corresponding Stokes numbers are 0.002, 0.2, 1.06, 3.7 and 11.9. Initial velocities of the particles are set to be equal to the local fluid velocities, ensuring that the particles are in dynamic equilibrium with the gas flow.

Fig. 6 shows the instantaneous vorticity pattern of the gas phase, and Fig. 7 shows the instantaneous distributions of the particles with different diameters at 500 nondimensional time. Distribution

of the 2 μm particles as shown in Fig. 7(a) resembles that of the vorticity structure of the gas flow shown in Fig. 6. The relaxation time of these small particles of extreme low Stokes number of 0.002 is much smaller than the gas time scale so that the particles have sufficient time to respond to the turbulence structure of the fluid flow. Hence the motion of small particles is fully controlled by the vortex structure of the gas phase and, as a result, many small particles manage to enter into the recirculation zones.

As the size of the particle increases, the effect of vortex on the particles becomes less efficient. Fig. 7(b) shows that 20 μm particles have the characteristic of preferential concentration along the boundary of the vortex structure [9] caused by stretching and folding [10]. The decreasing influence of vortex structure on particles of larger Stokes numbers is shown in Figs. 7(c)–(e). The Stokes numbers of all these particles are greater than unity and fewer particles are found in the recirculation zones. Most particles of the largest size in Fig. 7(e) can penetrate right through the vortex structure with little transverse dispersion. This is because particles with largest Stokes number have highest momentum and their motion is least influenced when the gas flow slows down or changes direction. It is however noted, even for the largest spheres, particles nearest to the backward-facing step are more likely driven into the recirculation zone because of the greatest velocity gradient of gas phase there.

In order to have better understanding of the dispersion effect of large-scale vortex on particles of different Stokes numbers, spheres of different diameters are introduced with same velocity and same position upstream of a vortex structure. Fig. 8 shows the behavior of particles when they pass through large vortices. Fig. 8(a) shows the dispersion of 2 μm particle. The particles follow closely with the fluid flow and the particle distribution pattern is very similar to the pattern of the vortex elements in the flow field. However, for increased particle diameters of 10, 20 and 50 μm as shown in Figs. 8(b)–(d), the vortex cores of the fluid are essentially devoid of particles, i.e. the particles are centrifuged out. The particles are concentrated within the extremely thin regions, outlining the boundaries of the large-scale vortex structures. For larger particles, there is even less mixing occurred and the particles are simply convected downstream with only a slight waviness detectable in their paths, as shown in Figs. 8(e) and (f).

In conclusion, particles with the smallest Stokes number ($St \ll 1$) are strongly controlled by the vortex structure of the gas phase and follow closely to the gas vortices. Such particles are not preferentially concentrated. Particles with time scales of similar order as the fluid time scale ($St \sim O(1)$) will be centrifuged out by a vortex and will be preferentially concentrated along the peripheral region of the vortex. Particles with large Stokes number ($St \gg 1$) are more persistent in maintaining their own movement. They do not essentially respond to the vortex motion within the fluid time scale available and will also not be preferentially concentrated.

5.4. *Effect of initial velocity slip*

Velocity slip is a measure of the velocity difference between the two phases. Depending on how particles are introduced into a channel, the initial velocity slip at the inlet always varies greatly with different real situations. It is therefore of interest to take into account the effect of initial velocity slip on particle dispersion through the vortex structures of the fluid. The inlet velocity slip is defined as $\alpha = U_{p0}/U_{f0}$, where U_{p0} and U_{f0} are the initial velocity of the particle phase and gas phase,

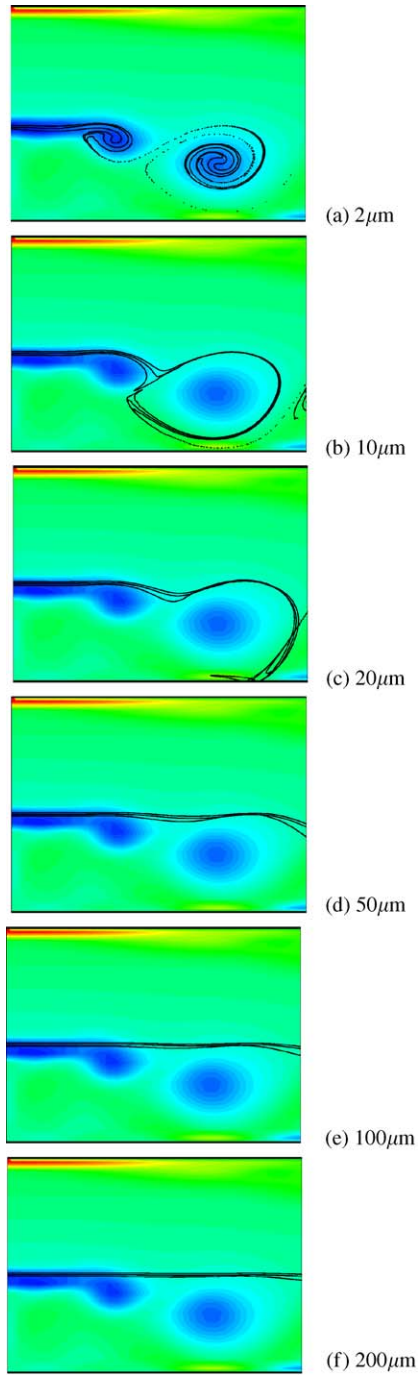

Fig. 8. The effect of large scale vortex on particle dispersion. (a) 2 μm, (b) 10 μm, (c) 20 μm, (d) 50 μm, (e) 100 μm (f) 200 μm.

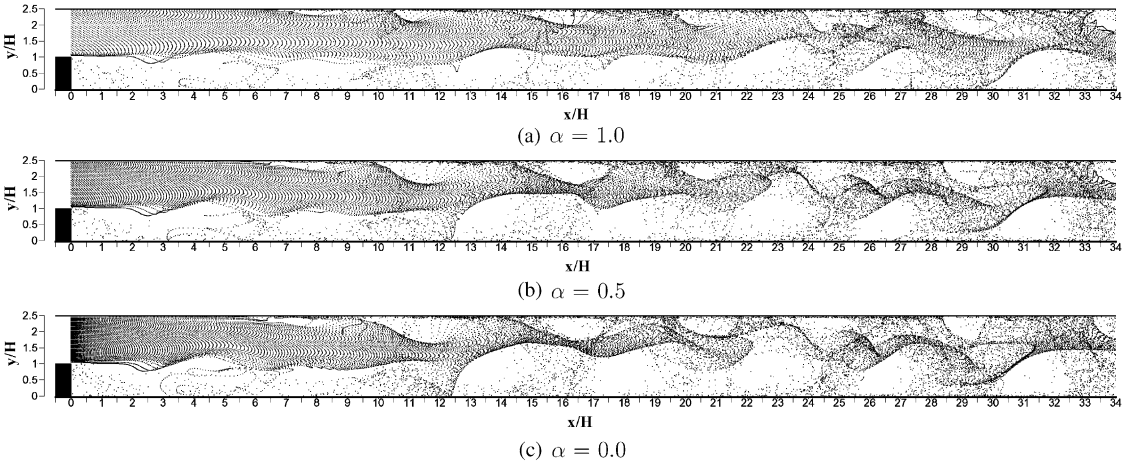

Fig. 9. Distribution of 100 μm particles with different initial velocity slips. (a) $\alpha = 1.0$, (b) $\alpha = 0.5$, (c) $\alpha = 0.0$.

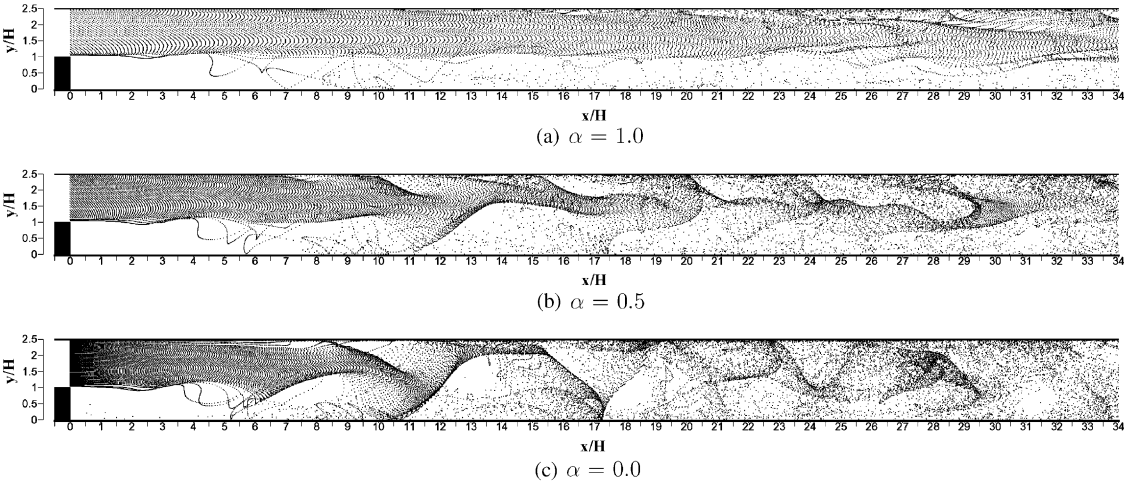

Fig. 10. Distribution of 200 μm particles with different initial velocity slips. (a) $\alpha = 1.0$, (b) $\alpha = 0.5$, (c) $\alpha = 0.0$.

respectively. When $\alpha = 0$, the particles are stationary when released into the flow, whereas for $\alpha = 1$ the particles are in dynamic equilibrium with the fluid.

Flows with initial velocity slip $\alpha = 1$, 0.5 and 0 are simulated in this paper. Numerical results reveal that although trajectories of small particles are strongly affected by the vortex structure of the gas phase, their distributions are insensitive to the change of initial velocity slips. Distributions of particles of diameter 2, 20, and 50 μm and with $\alpha = 0.5$ and 0 are similar to those with $\alpha = 1$ as shown in Figs. 7(a)–(c).

Fig. 9 shows the particles dispersion of 100 μm with different initial inlet velocity slips. Although the effect of vortex structures on the dispersion of large particles is relatively small, moderation becomes progressively significant as the slip reduces from $\alpha = 1$ to 0 as shown, respectively, in Figs. 9(a)–11(c). The lower or even zero initial momenta of the particles favor the transverse dispersion

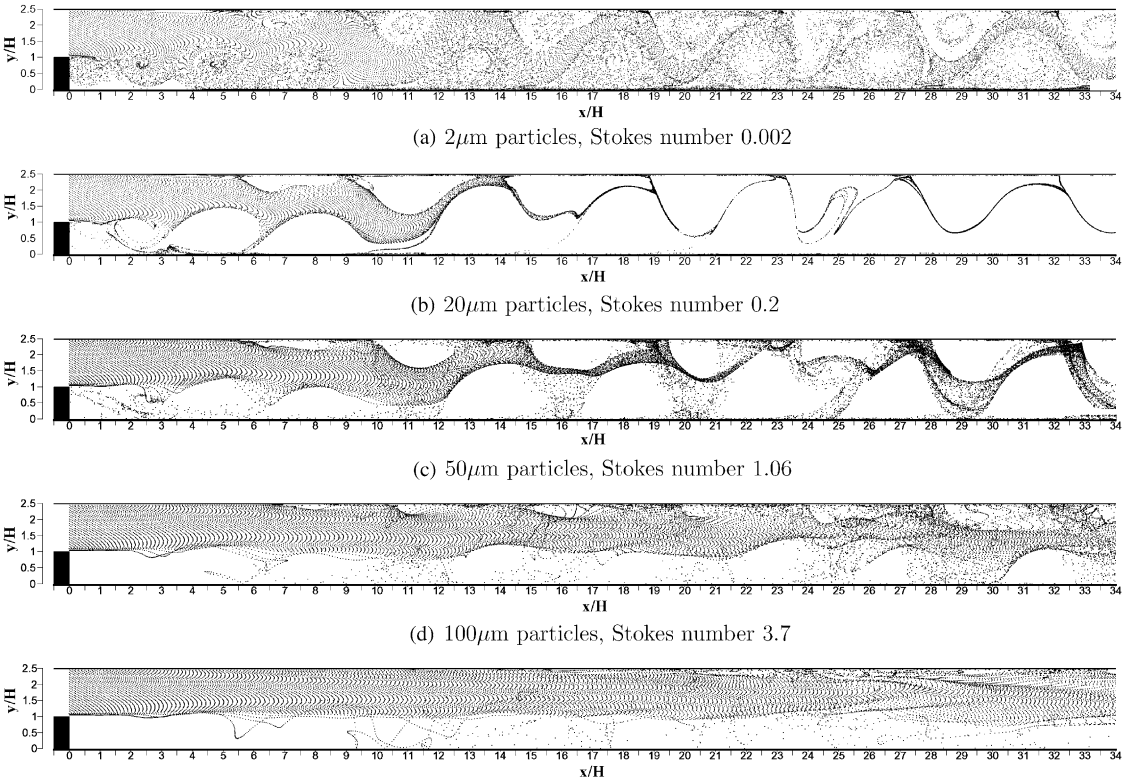

(a) 2μm particles, Stokes number 0.002

(b) 20μm particles, Stokes number 0.2

(c) 50μm particles, Stokes number 1.06

(d) 100μm particles, Stokes number 3.7

(e) 200μm particles, Stokes number 11.9

Fig. 11. Particle distribution of different particles with x-direction gravity. (a) 2 μm particles, Stokes number 0.002; (b) 20 μm particles, Stokes number 0.2; (c) 50 μm particles, Stokes number 1.06; (d) 100 μm particles, Stokes number 3.7; (e) 200 μm particles, Stokes number 11.9.

of the particles in the flow and the low or zero initial particle velocities result in a much longer time for the particles to respond to the fluctuating turbulence structure.

The dependence on initial velocity slip becomes more obvious for even larger particles of diameter 200 μm as shown in Fig. 10. With $\alpha=1$ shown in Fig. 10(a), particle trajectories essentially maintain their initial direction downstream, apart from a few particles near the step that migrate into the recirculation area because of the great velocity gradient of gas phase there. However, smaller velocity slips result in relatively greater transverse dispersion of particles as shown in Figs. 10(b) and (c).

5.5. *Effect of gravity on particle dispersion*

Gravitational force is introduced in x- and y-directions, respectively, in order to compare the effect of gravity on particle dispersion with different diameters. The particles are initially set in dynamic equilibrium with the fluid when they are released into the fluid flow.

According to the simulation results, dispersions of all tested particles are insensitive to the gravity effect when its direction is along the x-axis. This is why experimental channels of similar two phase flows is always set in a vertical direction in order to minimize the effect of gravity. Fig. 11 shows

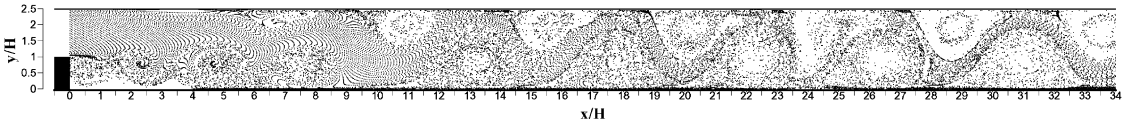

(a) 2μm particles, Stokes number 0.002

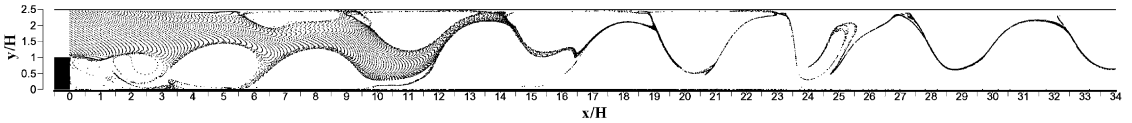

(b) 20μm particles, Stokes number 0.2

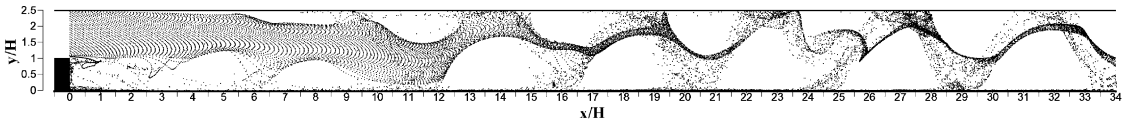

(c) 50μm particles, Stokes number 1.06

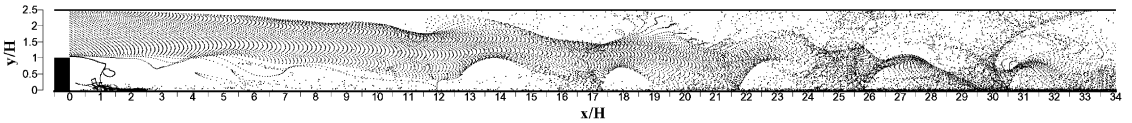

(d) 100μm particles, Stokes number 3.7

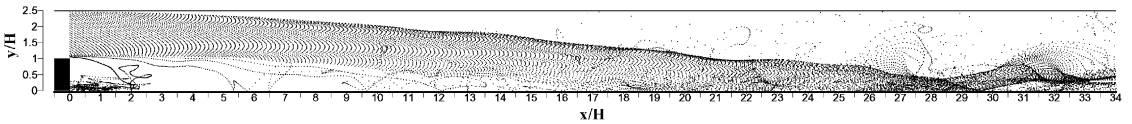

(e) 200μm particles, Stokes number 11.9

Fig. 12. Particle distribution of different particles with y-direction gravity. (a) 2 μm particles, Stokes number 0.002; (b) 20 μm particles, Stokes number 0.2; (c) 50 μm particles, Stokes number 1.06; (d) 100 μm particles, Stokes number 3.7; (e) 200 μm particles, Stokes number 11.9.

the dispersion of particle with different Stokes numbers. They show the similar patterns as those shown in Fig. 7 of the simulated particles under no gravity force.

Figs. 12(a)–(c) illustrate that the dispersion process of particles for $St \ll 1$ and $St \sim O(1)$ is insensitive to the y-direction gravity effect. The 100 μm particles exhibit small transverse displacement due to y-direction gravity as shown in Fig. 12(d). A sharp contrast occurs for particles with $St \sim 10$ as shown in Fig. 12(e). Progressive lateral sedimentation occurs in the lower section of the channel.

6. Conclusions

In the present study, numerical simulation of two-phase turbulent flow over a backward-facing step has been successfully investigated by large eddy simulation (LES) for the gas phase and a Lagrangian method with particle tracking model for the particle phase.

Particle tracking method and one-way coupling assumption are effective in predicting the particles flow. Velocity profiles of two types of particles have been predicted and found to be in good agreement with experimental results. Simulation has also successfully demonstrated the preferential

concentration of particles in the flow. Preferential concentration is one of the important phenomena of particle dispersion in turbulent flow. It leads to a very nonuniform distribution of particles and is an important factor to consider in practical applications.

Simulation results show that dispersion of particles with Stokes numbers in the range of $St \ll 1$ and $St \sim O(1)$ are insensitive to the change of initial velocity slips. However, for particles of Stokes number much greater than one, decreasing of initial two phase velocity slip plays a significant role in the relative enhancement of transverse dispersion of particles. Therefore, the design of initial conditions of the particle phase has an important influence on particle distribution in the flow. This suggests that a proper choice of particle feeding mechanism is important to the ensuing flow pattern of the particles.

Numerical results show the dispersions of all tested particles are insensitive to the effect of x-direction gravity, i.e., along the direction of the main stream. This is why the backward facing step channel is set in a vertical direction in the experiment in order to reduce the gravitational effect. Under a traversed gravitational field, particles with $St \ll 1$ and $St \sim O(1)$ are also insensitive to the y-direction gravity. However, y-direction gravity effect will significantly change the dispersion of particles for $St \sim 10$ or larger. Progressive lateral sedimentation occurs downstream of the channel.

Acknowledgements

This work was partially supported by the Research Committee of The Hong Kong Polytechnic University (Project No. G-W029) and a grant from the Research Grants Council of the Hong Kong Special Administrative Region (Project No. PolyU 5150/02E (B-Q554)).

References

[1] K. Akselvoll, P. Moin, Large-eddy simulation of turbulent confined coannular jets, J. Fluid Mech. 315 (1996) 387–411.
[2] B.L. Buzbee, G.H. Golub, C.W. Nielson, On direct methods for solving Poisson's equations, SIAM J. Numer. Anal. 7 (1970) 627–656.
[3] C.K. Chan, H.Q. Zhang, K.S. Lau, Numerical simulation of gas-particle flows behind a backward-facing step using an improved stochastic separated flow model, Comput. Mech. 27 (5) (2001) 412–417.
[4] A.J. Chorin, Numerical solution of the Navier–stokes equations, Math. Comput. 22 (1968) 745–762.
[5] L.S. Fan, C. Zhu, Principles of Gas–Solid Flows, Cambridge University Press, New York, 1996, p. 87.
[6] J.R. Fessler, J.K. Eaton, Turbulence modification by particles in a backward-facing step flow, J. Fluid Mech. 314 (1999) 97–117.
[7] H. Le, P. Moin, J. Kim, Direct numerical simulation of turbulent flow over a backward-facing step, J. Fluid Mech. 330 (1997) 349–374.
[8] J. Smagorinsky, General circulation experiments with primitive equations, Monthly Weather Rev. 91 (1963) 99–164.
[9] K.D. Squires, J.K. Eaton, Preferential concentration of particles by turbulence, Phys. Fluids A—Fluid Dyn. 3 (5) (1991) 1169–1179.
[10] L. Tang, F. Wen, Y. Yang, C.T. Crowe, J.N. Chung, T.R. Troutt, Self-organizing particle dispersion mechanism in a plane wake, Phys. Fluids A—Fluid Dyn. 4 (10) (1992) 2244–2251.
[11] F.O. Thomas, Structure of mixing layers and jets, Appl. Mech. Rev. 44 (3) (1991) 119–153.